Mineralogical Magazine, February 2003, Vol. 67(1), pp. 95–102

Paragenesis and mineral chemistry of alabandite (MnS) from the Ag-rich Santo Toribio epithermal deposit, Northern Peru

G. R. Olivo* and K. Gibbs†

Department of Geological Sciences and Geological Engineering, Queen's University, Kingston, Ontario, Canada K7P 2L7

ABSTRACT

The Miocene, epithermal, Ag-rich polymetallic Santo Toribio deposit is hosted by the volcanics of the Quiruvilva-Pierina subbelt, Northern Peru, which also comprises the world-class, high sulphidation Pierina deposit. The Ag-rich, alabandite-bearing veins of the Santo Toribio deposit formed during two major stages. The early stage is characterized by deposition of arsenopyrite, pyrite, quartz, Mn-sphalerite, stannite, alabandite and minor miargyrite. Sphalerite associated with this stage is exceptionally enriched in Mn (up to 14.5 wt.%) and alabandite is optically and mineralogically zoned. Its brown zones have greater Fe+Sb and smaller Mn contents than the green zones and Fe+Sb replaces Mn in its structure. During this early stage, f_{S_2} must have been high to allow the stabilization of alabandite relative to rhodochrosite. In the second stage, the physicochemical conditions changed and the CO_2/S ratio increased, causing dissolution of alabandite and the deposition of abundant rhodochrosite and a second generation of arsenopyrite, pyrite and quartz, sphalerite with chalcopyrite inclusions, mirargyrite, ramdohrite, and finally stibnite. This polymetallic ore probably formed due to an abrupt decrease in H^+ and/or Cl^- concentration caused by boiling or dilution of the high-salinity hydrothermal fluids and constitutes an example of "intermediate sulfidation-state" epithermal deposits.

Keywords: alabandite, Santo Toribio epithermal deposit, Peru.

Introduction

Alabandite, which is an isometric manganese sulphide dimorphic with rambergite (MnS, hexagonal), occurs in a diversity of geological settings, including Mn-rich sedimentary rocks (Vassileff, 1987; Mücke *et al*., 1999), veins in contact-metamorphosed Mn-rich sedimentary rocks and/or skarns (Törnroos, 1982; Dobbe, 1992; Ragu, 1994), Pb-Zn-Ag replacement deposits in carbonate sequences (Hewett and Rove, 1930), mesothermal veins in pyrite-rich sedimentary rocks (Graham, 1978), Ag-rich polymetallic volcanic-hosted epithermal deposits (Hewett and Rove, 1930; Burbank, 1933), and meteorites (Skinner and Luce, 1971).

Although alabandite has been commonly reported in sediment-hosted ores, little information is available on its mode of occurrence and paragenesis in Ag-rich volcanic-hosted, epithermal deposits and there are no data on its mineral chemistry in this environment. We present in this paper, the results of a detailed petrographic and mineral chemistry investigation of alabandite and its associated vein minerals from the Ag-rich Santo Toribio epithermal deposit, to further our understanding of the processes responsible for the formation of Mn- and Ag-rich polymetallic ore in volcanic-hosted epithermal systems.

* E-mail: olivo@geol.queensu.ca
DOI: 10.1180/0026461036710087
† Present address: SGS Lakefield Research Limited, P.O. Box 4300, 185 Concession Street, Lakefield, Ontario, Canada K0L 2H0

Mode of occurrence and paragenesis

The Santo Toribio ore is a low-sulphidation epithermal Ag-rich polymetallic deposit hosted

in the Quiruvilva-Pierina subbelt, which also contains the world-class, high sulphidation Pierina deposit (Noble and McKee, 1999). Both deposits are hosted by upper Oligocene-middle Miocene andesitic to rhyolitic, subaerial, volcanic rocks of the upper Calipuy Group (also referred to as the Huaraz Group), and formed between 16.5 to 13.3 Ma (Strusievicz *et al*., 2000).

The Santo Toribio deposit is regionally controlled by NW–SE-trending lineaments (Chamorro, 1984) and has been intermittently mined since 1951. It comprises NW-, NE- and EW-striking quartz and/or carbonate veins (up to 220 m in length; Chamorro, 1984) with variable proportions of sulphides, mainly pyrite, arsenopyrite, sphalerite and alabandite. The Ag and Au grades in the polymetallic ore average 744 and 3 g/t, respectively (Vachon, 1999), yielding a Ag/Au ratio in the order of 10^2–10^3:1. Alabandite-rich veins contain the highest Ag grade (up to 1360 g/t Ag and 1.63 g/t Au) and comprise three main layers and irregular patches, which are (Fig. 1*a*): (a) alabandite-rich (up to 40 vol.%), (b) coarse-grained carbonate-quartz (up to 55 vol.%) and (c) fine-grained quartz-pyrite (~5 vol.%).

The alabandite-rich layer (Fig. 1*a–f*) is brecciated and composed of fractured and corroded grains of alabandite (up to 85 vol.% of the layer), euhedral quartz crystals, rhodochrosite, pyrite, arsenopyrite, Mn-bearing sphalerite, stannite (Cu_2FeSnS_4), ramdohrite ($Ag_3Pb_6Sb_{11}S_{24}$), miargyrite ($AgSbS_2$) and stibnite (Sb_2S_3). Alabandite grains exhibit complex, concentric green and brown zones (Fig. 1*b*) and contain inclusions of arsenopyrite, pyrite, quartz (Fig. 1*c*), composite Mn-sphalerite-stannite grains (Fig. 1*d,f*), and miargyrite, evenly distributed in both zones. Miargyrite inclusions are found in sharp contact with Mn-sphalerite-stannite grains (Fig. 1*d*) or as isolated grains (Fig. 1*e*). Mn-sphalerite-stannite grains include pyrite and arsenopyrite. Corroded rims and fractures in alabandite are filled mainly with rhodochrosite, pyrite, and minor miargyrite (Fig. 1*a,e,f*) and ramdohrite. Euhedral quartz crystals, commonly with pyrite inclusions, occur interstitial to corroded alabandite grains and are mantled by rhodochrosite. Stibnite occupies fractures and embayments in rhodochrosite and sphalerite.

Quartz-pyrite layers are composed of irregular quartz grains with interstitial carbonate (80 vol.%), euhedral to irregular shaped pyrite I and arsenopyrite I grains (up to 40 μm in diameter and averaging 15 vol.%). Minor stibnite and sphalerite (with chalcopyrite inclusions) mantle or fill corroded rims of pyrite I and arsenopyrite I. These layers are rare and occur locally between the alabandite-rich and carbonate-quartz layers (Fig. 1*a*).

The carbonate-quartz layers contain coarse-grained rhodochrosite commonly in the core of the layer, and euhedral crystals of quartz in the rim (Fig. 1*a*). Quartz crystals are oriented with the long axes perpendicular to the layer boundary, and contain inclusions of pyrite and arsenopyrite. Miargyrite (Fig. 1*g*) and sphalerite with abundant inclusions of chalcopyrite occur as isolated irregular grains and sphalerite locally fills corroded zones in pyrite II (Fig. 1*h*). Supergene manganite and goethite (Fig. 1*g*) locally occupy fractures and corroded zones in rhodochrosite, pyrite and sphalerite.

Based on the textural relationships described above, the following paragenetic sequence has been proposed for the Mn-rich hydrothermal ore of the Santo Toribio deposit (Fig. 2). The first phases that started to precipitate were pyrite I and arsenopyrite I, which commonly occur included in other minerals. Subsequently, alabandite, quartz, Mn-sphalerite-stanite, and minor miargyrite were deposited, followed by arsenopyrite II, pyrite II

FIG. 1. Photomicrographs of the alabandite-bearing vein. (*a*) The three major layers: alabandite-rich (left), quartz-pyrite (QPL, centre) and carbonate-quartz (right) (reflected light). (*b*) Concentric green and brown zones in fractured and corroded alabandite grains (transmitted, plain-polarized light). (*c*) Quartz, pyrite and arsenopyrite included in alabandite (reflected light). (*d*) Stannite, sphalerite and miargyrite included in alabandite (reflected light). (*e*) Alabandite grains with an inclusion of miargyrite and corroded rims and fractures filled with rhodochrosite, pyrite and miargyrite (reflected light). (*f*) Alabandite with inclusions of composite grains of stannite-sphalerite. Note interstitial quartz grains and rhodochrosite and pyrite filling fractures and embayments in alabandite (reflected light). (*g*) Miargyrite interstitial to rhodochrosite in carbonate-quartz layer (reflected light). (*h*) Corroded pyrite grains filled with sphalerite and stibnite (reflected light). Ald = alabandite, Aspy = arsenopyrite, Cpy = chalcopyrite, Goe = goethite, Mi = miargyrite, Mnt = manganite, Py = pyrite Qz = quartz, Rd = rhodochrosite, Sph = sphalerite, Stb = stibnite, Stn = stannite (II denotes second generation).

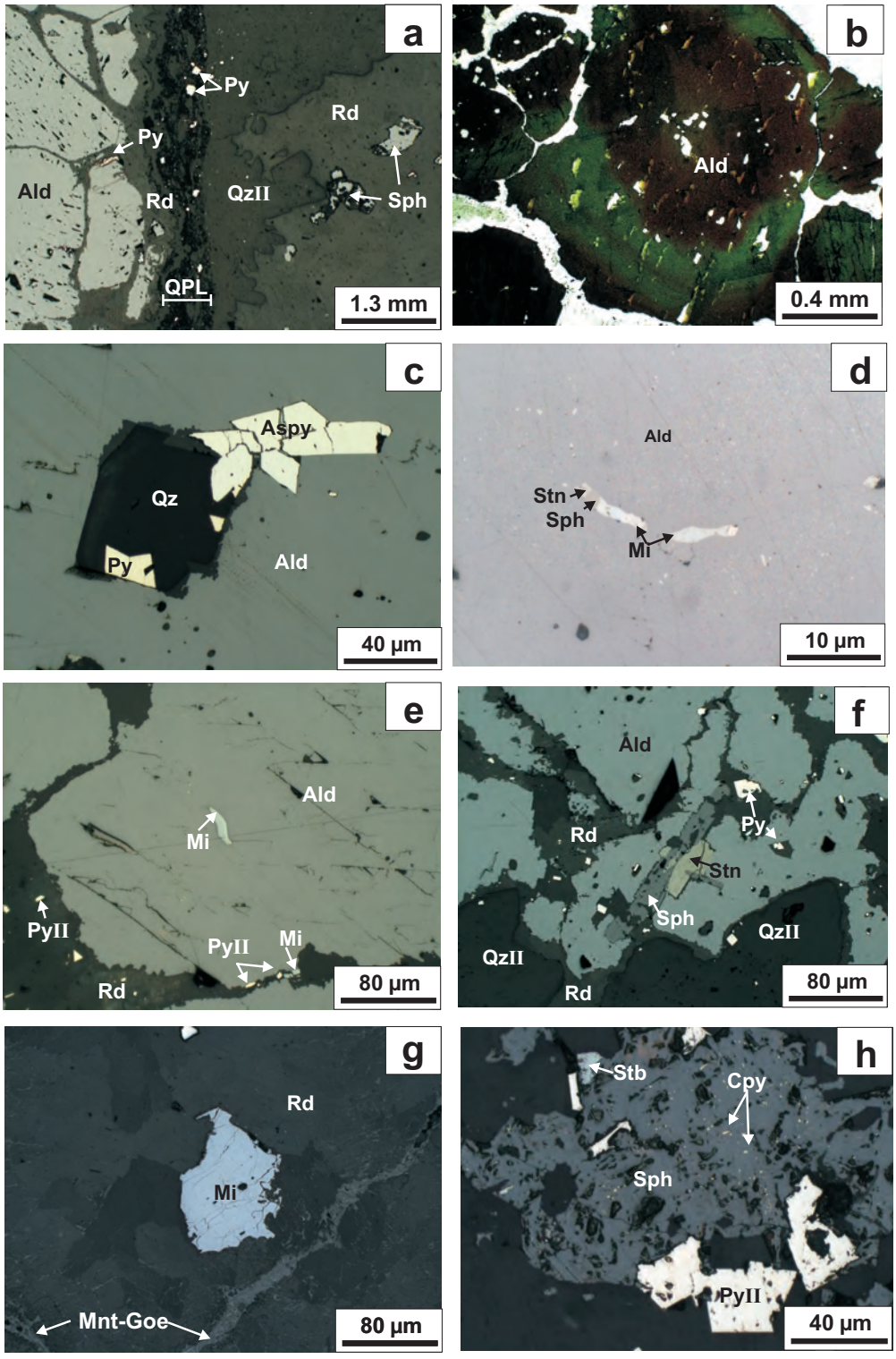
a
Py
Py
Rd
Ald
Rd
QzII
Sph
QPL
1.3 mm
b
Ald
0.4 mm
c
Aspy
Qz
Py
Ald
40 µm
d
Ald
Stn
Sph
Mi
10 µm
e
Ald
Mi
PyII
PyII
Mi
Rd
80 µm
f
Ald
Py
Rd
Stn
Sph
QzII
QzII
Rd
80 µm
g
Rd
Mi
Mnt-Goe
80 µm
h
Stb
Cpy
Sph
PyII
40 µm

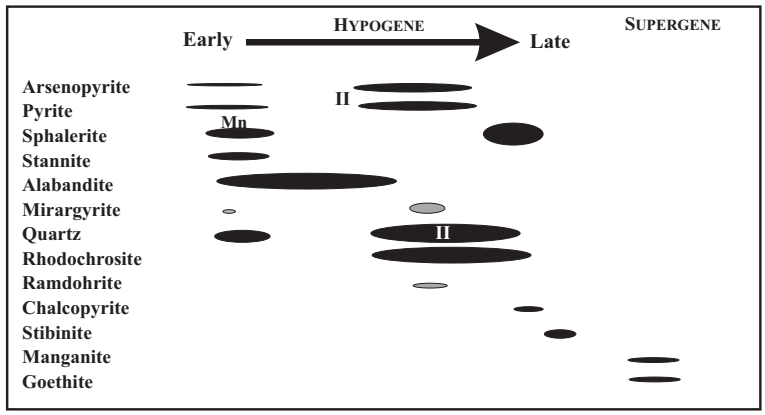

FIG. 2. Paragenetic sequence for the alabandite-bearing veins from Santo Toribio.

and quartz, rhodochrosite, sphalerite with chalcopyrite inclusions, mirargyrite, ramdohrite and finally, stibnite.

Mineral chemistry

Quantitative analyses of minerals of the Mn- and Ag-rich Santo Toribio ore were conducted using the Jeol JXA-8900L automated wavelength-dispersion electron microprobe (EMP) at McGill University in Montreal. The analyses were conducted with an accelerating voltage of 20 kV and a beam current of 30 nA. Beam diameters of 10 μm and 5 μm were used for analysis of carbonate and sphalerite, respectively, and of 2 μm for mirargyrite and alabandite. Carbonate analysis was calibrated using internal standards of dolomite (CaO and MgO), strontianite (SrO) and siderite (FeO and MnO). The standards used for calibration for the analysis of the sulphide minerals include: spessartine (Si, Mn and Al), diopside (Mg), $AgBiSe_2$ (Ag), CanMet ZnS (Zn and S), CanMet pyrite (Fe and S), CanMet stibnite (Sb) and CanMet pentlandite (Ni).

Electron microprobe data were collected from 206 points along straight lines across four concentrically zoned alabandite grains (Table 1) and single element scans for Mn, S, Fe and Sb were conducted in selected grains (Fig. 3) in order

TABLE 1. Composition of alabandite from the Santo Toribio deposit.

	Green zones (N = 96)		Brown zones (N = 113)	
	Range	Mean	Range	Mean
Wt.%*				
Mn	61.6–62.9	62.3	59.8–62.7	61.0
Fe	0.0–1.0	0.3	0.3–2.6	1.4
Sb	0–0.3	0.1	0–1.2	0.3
S	35.9–36.7	36.3	35.2–36.6	36.3
a.p.f.u.#				
Mn	0.986–1.006	0.999	0.960–1.002	0.978
Fe	0.0–0.016	0.004	0.004–0.042	0.022
Sb	0.0–0.002	0.00	0.00–0.008	0.002
Σ		1.003		1.002
S	0.988–1.002	0.997	0.988–1.004	0.998

* Ag, Al, Ca, Mg, Ni, Zn were also analysed and were not detected or are lower than 0.1 wt.%
# The atomic proportions are based on 2 atoms per formula unit (a.p.f.u.)

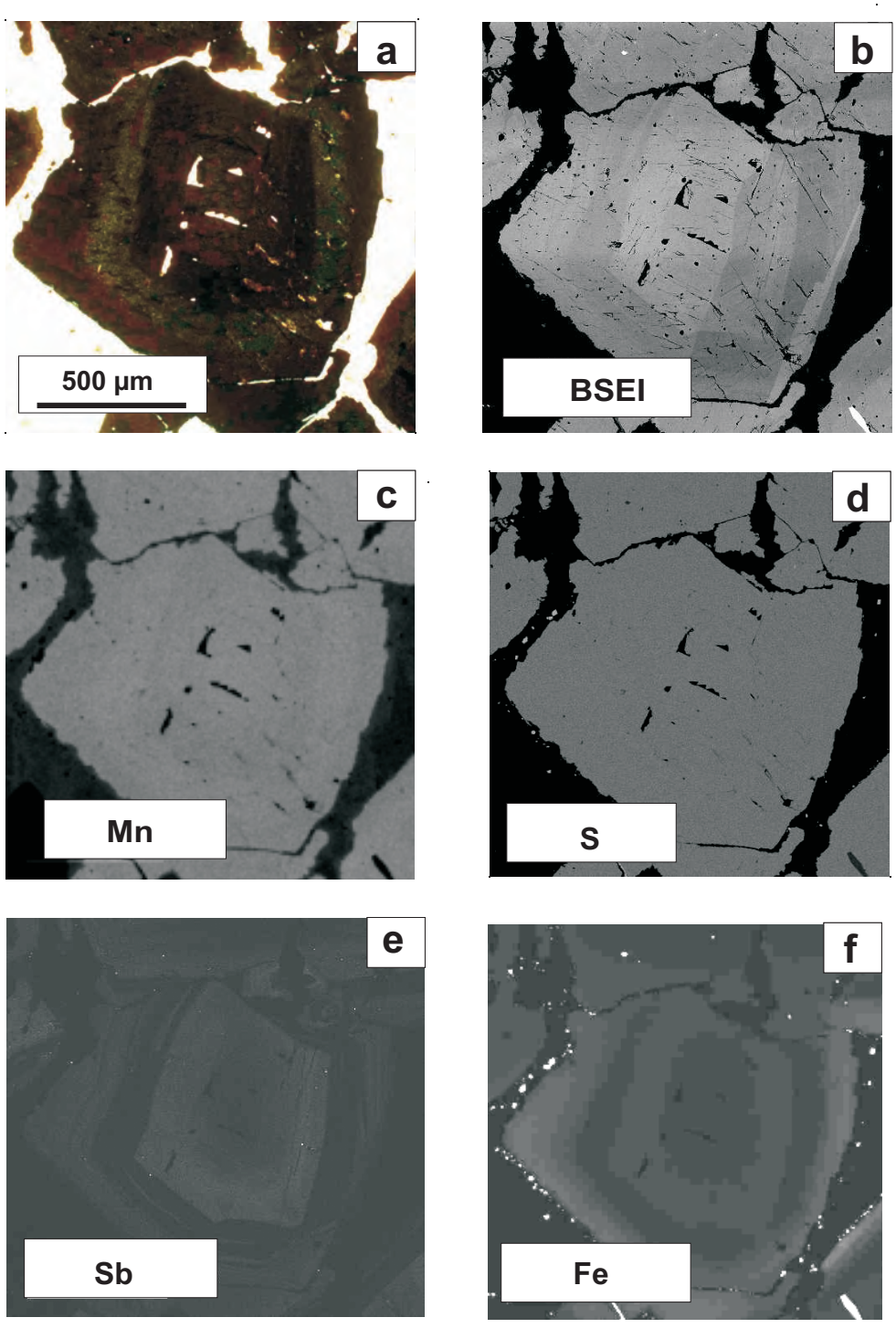

FIG. 3. (*a*) Photomicrograph of the alabandite grain selected for single-element scanning. (*b*) Back-scattered electron image of the selected grain. (*c,d,e,f*) Single element scans for Mn, S, Sb and Fe, respectively.

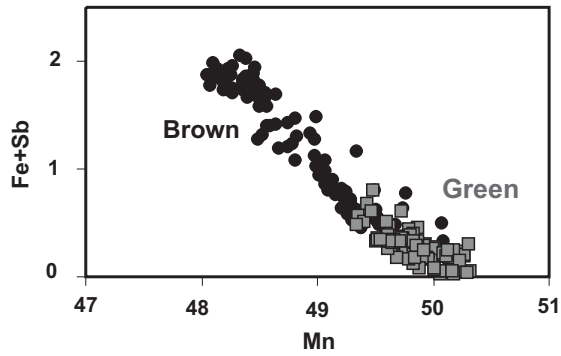

FIG. 4. A plot of Mn *vs*. Fe+Sb (in atomic proportions), comparing the composition of the green (squares) and brown (circles) zones in alabandite.

to document the variation of their composition. The results reveal that alabandite contains minor amounts of Fe and Sb and the brown zones have higher Fe + Sb and lower Mn contents than the green zones (Fig. 3). Manganese correlates negatively with Fe+Sb in the brown zones (correlation coefficient: R^2 = 0.91; Fig. 4), suggesting that Mn is replaced by Fe+ Sb. In the green zones, this correlation is less evident (R^2 = 0.53), probably because Fe and Sb contents are near background levels in most of the analyses. This is the first time that Sb has been reported in alabandite.

Sphalerite, previously referred to as Mn-sphalerite, forms composite grains with stannite and contains up to 14.5 and 5 wt.% Mn and Fe, respectively (Table 2). Zinc correlates negatively with Mn+Fe (R^2 = 0.97) indicating that it is replaced by Mn+Fe. Based on this assumption and using the average composition, the Mn-sphalerite formula was calculated as $(Zn_{0.70}Mn_{0.23}Fe_{0.08})_{\Sigma 1.01}S$. To our knowledge, this is the highest Mn content in sphalerite reported in the literature. Mirargyrite analyses yielded (wt.%): 36.78 Ag, 40.74 Sb and 21.24 S and rhodochrosite contains on average (mol.%) 77.7 $MnCO_3$, 20.0 $CaCO_3$, 1.9 $MgCO_3$ and 0.4 $FeCO_3$.

Energy-dispersive spectral analyses were also conducted on ramdohrite, stibnite, stannite and pyrite II in the alabandite-rich layer. These

TABLE 2. Composition of Mn-sphalerite from the alabandite-rich layer.

Wt.%	1	2	3	4	5	6	7	8	9	10	11	12
Zn	49.02	47.90	47.55	46.99	48.99	49.39	48.00	47.96	50.02	47.19	47.36	47.85
Mn	12.12	13.47	13.79	14.49	12.19	12.01	13.55	13.40	12.27	13.49	13.53	13.10
Fe	4.26	4.61	4.87	4.78	4.12	3.95	3.99	3.89	3.83	5.01	4.87	4.92
S	33.44	33.38	33.91	34.01	33.46	33.44	33.24	33.30	33.63	33.12	33.63	33.52
Total	98.84	99.36	100.12	100.27	98.76	98.79	98.78	98.55	99.75	98.81	99.39	99.39
a.p.f.u.[#]												
Zn	0.718	0.698	0.686	0.676	0.717	0.725	0.705	0.703	0.727	0.691	0.687	0.696
Mn	0.211	0.233	0.236	0.247	0.212	0.209	0.236	0.233	0.211	0.234	0.234	0.226
Fe	0.073	0.078	0.082	0.080	0.071	0.067	0.068	0.066	0.065	0.086	0.083	0.084
Σ	1.002	1.009	1.004	1.003	1.001	1.001	1.007	1.003	1.003	1.011	1.004	1.006
S	0.998	0.991	0.996	0.997	1.000	0.999	0.993	0.997	0.997	0.989	0.996	0.994

*Ag, Al, Mg, Sb and Si were also analysed and were not detected or are <0.1 wt.%
[#] The atomic proportions are based on 2 atoms per formula unit (a.p.f.u.)

analyses were valuable in confirming their optical identification and showed that Mn is a common minor element in all of these phases.

Discussion

The detailed petrographic and mineral chemistry investigation of the Mn-rich ore of the Santo Toribio deposit demonstrated that it is a polymetallic system with Fe, Zn, Cu, Pb, Mn, Sn, Ag, S and Sb-bearing minerals. Two major stages of ore formation were identified: the early one is characterized by the stability of alabandite and the later one by partial dissolution of alabandite and precipitation of rhodochrosite. The compositional zoning of alabandite, with Fe+Sb replacing Mn, indicates that the physicochemical conditions oscillated during its deposition. During the early stage, f_{S_2} must have been high to allow the stabilization of alabandite relative to rhodochrosite, according to reaction 1: $2MnS + 2CO_2 + O_2 = 2MnCO_3 + S_2$ and according to Krauskopf and Bird (1995).

In addition, Sb concentration was probably relatively high as inferred by its incorporation in alabandite zones and the precipitation of a silver antimonide (miargyrite). In the second stage, the physicochemical conditions changed and the CO_2/S ratio increased, causing deposition of abundant rhodochrosite that partially replaced alabandite (reaction 1). Significantly, Ag-, Pb- and Sb-bearing minerals (i.e. miargyrite, ramdohrite and stibnite) are more common in rhodochrosite layers and patches.

Epithermal, Mn-rich polymetallic veins with a high Ag/Au ratio, similar to the samples investigated here, may have been formed by high-salinity fluids (Henley, 1985; Gammons and Seward, 1996), which are favourable for transporting Mn and Ag as Cl complexes. In these systems, the Ag/Au ratio is high because Au does not form stable chloride complexes (Gammons and Williams-Jones, 1995). In high-salinity fluids, at temperatures lower than 300ºC, rhodochrosite may have precipitated due to an abrupt decrease in H^+ and/or Cl^- concentration, which may be caused by boiling or dilution of the hydrothermal fluids (Gammons and Seward, 1996). These changes would also cause the precipitation of Ag, according to reaction 2: $Ag_{(s)} + 2Cl^- + H^+ + ¼O_{2(g)} = AgCl_2^- + ½H_2O$ (Gammons and Williams-Jones, 1995), which explains the occurrence of Ag-bearing minerals associated with rhodochrosite.

Implications for exploration

The geological setting and the mineral assemblage of the Mn-rich ore of the Santo Toribio deposit are similar to the subset of low-sulphidation epithermal deposits, defined as "intermediate sulphidation-state" (Hendenquist *et al*., 2000). The Santo Toribio deposits and the intermediate sulphidation-state deposits are hosted by andesite-rhyodacite-rhyolitic sequences, are Ag-, Mn- and base metal-rich, have high Ag/Au ratio, and occur in belts that host high-sulphidation deposits. Because both high-sulphidation and intermediate-sulphidation-state epithermal deposits are commonly associated with porphyry deposits (e.g. Lepanto District; Hendenquist *et al*., 2000), the Quiruvilva-Pierina subbelt, which has traditionally been explored for epithermal Au-Ag deposits, should also be explored for porphyry Cu deposits.

Acknowledgements

We are grateful to G. Poirier, McGill University, R. Mineau, Université du Québec à Montréal, D. Kempson and N. Bursztyn, Queen's University, for assistance during quantitative and qualitative analyses using the electron microprobe, scanning electron microscope and X-ray diffration. We also thank A. Clark, A. Rainbow, R. Strusievicz and A. Vachon for discussions on the Quiruvilva-Pierina subbelt and for sharing their sample with us. The manuscript benefited from reviews by D. Love, P. Roeder and an anonymous reviewer. This research was supported by research and infrastructure grants from the Natural Sciences and Engineering Research Council of Canada, Canadian Foundation for Innovation and Ontario Innovation Trust to G. Olivo.

References

Burbank, W.S. (1933) The manganese minerals of the Sunnyside veins, Eureka Gulch, Colorado. *American Mineralogist*, **18**, 513–527.

Chamorro, C.E., (1984) *Peru: A Mining Country*. INGEMMET, Ore Deposits **4a**, 490–503.

Dobbe, R.T.M. (1992) Manganoan-cadmian tetrahedrite from the Tunaberg Cu-Co deposit, Bergslagen, central Sweden. *Mineralogical Magazine*, **56**, 113–115.

Gammons, C.H. and Seward, T.M. (1996) Stability of manganese (II) chlorite complexes from 25 to 300ºC.

Geochimica et Cosmochimica Acta, **60**, 4295–4311.

Gammons, C.H. and Williams-Jones, A.E. (1995) Solubility of Au-Ag alloy + AgCl in HCl/NaCl solutions at 300ºC. *Geochimica et Cosmochimica Acta*, **59**, 1655–1668.

Graham, J. (1978) Manganochromite, palladium antimonide, and some unusual mineral associations at the Nairne pyrite deposit, South Australia. *American Mineralogist*, **63**, 1166–1174.

Hendenquist, J.W., Arribas, A.R. and Gonzalez-Urien, E. (2000) Exploration for epithermal gold deposits. In *Gold in 2000* (S.G. Hagemann and P.E. Brown, editors). *Reviews in Ecomomic Geology*, **13**, 245–277.

Hewett, D.F. and Rove, O. N. (1930) Occurrence and relations of alabandite. *Economic Geology*, **25**, 36–56.

Krauskopf, K.B. and Bird, D.K. (1995) *Introduction to Geochemistry*, third edition. WCB McGraw-Hill, Boston, pp. 364–597.

Mücke, A., Dzigbodi-Adjimah, K. and Annor, A. (1999) Mineralogy, petrography and genesis of the Paleoproterozoic Birimian manganese-formation of Nsuta/Ghana. *Mineralium Deposita*, **34**, 297–311.

Noble, D.C. and McKee, E.H. (1999) The Miocene metallogenic belt of central and northern Peru. Pp. 155–193 in: *Geology and Ore Deposits of the Central Andes* (B.J. Skinner, editor). Special Publication **7**, Society of Economic Geology.

Ragu, A. (1994) Helvite from the French Pyrénees as evidence for granite-related hydrothermal activity. *The Canadian Mineralogist*, **32**, 111–120.

Skinner, B.J. and Luce, F.D. (1971) Solid solutions of the type (Ca, Mg, Mn, Fe)S and their use as geothermometers for the enstatite chondrites. *American Mineralogist*, **56**, 1269–1297.

Strusievicz, O.R., Clark, A., Lee, J.K.L. and Farrar, E. (2000) Metallogenetic relationships of the Huaraz, Ancash, segment of the precious-base metal subprovince of Northern Peru. *Abstracts with Program Geological Society of America Annual Meeting*, p. 504.

Törnroos, R. (1982) Properties of alabandite; alabandite from Finland. *Neues Jahrbuch für Mineralogie Abhanlungen*, **144**, 107–123.

Vachon, A. (1999) *New gold discovery near the Pierina mine in Peru*. Sulliden Exploration Inc. Public Press Release, September 1999, Montreal, Quebec, Canada.

Vassileff, L. (1987) L'alabandite du gîte stratiforme d'obrochishté (Varna, Bulgarie). *Comptes rendus du Congres National des Societes Savantes*, **112**, 217–224.

[*Manuscript received 7 August 2002: revised 19 December 2002*]